

# Evaluation of the Telescope Array surface detector's energy reconstruction performance using a deep neural network and hybrid data

**Anton Prosekin,<sup>a,\*</sup> Kozo Fujisue,<sup>a</sup> Anatoli Fedynitch<sup>a,b</sup> and Hiroyuki Sagawa<sup>b</sup> on behalf of the Telescope Array Collaboration**

<sup>a</sup>*Institute of Physics, Academia Sinica,  
Taipei, Taiwan*

<sup>b</sup>*Institute for Cosmic Ray Research, The University of Tokyo,  
Tokyo, Japan*

*E-mail: [antonpr@gate.sinica.edu.tw](mailto:antonpr@gate.sinica.edu.tw), [kfujisue@gate.sinica.edu.tw](mailto:kfujisue@gate.sinica.edu.tw),  
[anatoli@gate.sinica.edu.tw](mailto:anatoli@gate.sinica.edu.tw), [hsagawa@icrr.u-tokyo.ac.jp](mailto:hsagawa@icrr.u-tokyo.ac.jp)*

Accurate reconstruction of Ultra-High-Energy Cosmic Ray (UHECR) parameters is crucial for understanding their origins and composition. We present a newly developed Deep Neural Network (DNN) approach based on the AixNet architecture for reconstructing UHECR parameters from Telescope Array surface detector (SD) data. This model reconstructs key parameters, including energy, arrival direction, core position,  $X_{max}$ , and primary mass, by analyzing time traces and spatial correlations. Monte Carlo simulations for four mass groups (proton, helium, CNO, and iron) demonstrate that the DNN improves the resolution of energy and core position while achieving comparable resolution for arrival direction compared to standard reconstruction methods. We expect that the DNN will achieve these improvements with looser data quality requirements, potentially increasing the available event statistics. We provide expected resolution figures and systematic studies from simulations and validate the DNN's performance using hybrid data.

*7th International Symposium on Ultra High Energy Cosmic Rays (UHECR2024)  
17-21 November 2024  
Malargüe, Mendoza, Argentina*

---

\*Speaker

## 1. Introduction

Despite growing observational data, the sources of UHECR remain unknown. The propagation of UHECR is a complex interplay between energy losses, nuclei photodissociation, and deflection. Its modeling requires accurate knowledge of the energies, particle types, and arrival directions of detected particles. Due to low fluxes and extreme energies, UHECR are observed indirectly through extensive air showers, making primary particle reconstruction a complex inverse problem. Standard approaches rely on phenomenological models fitted to observations [1, 2], but they use approximations, which may reduce accuracy. DNNs offer a powerful alternative, handling high-dimensional data and capturing complex relationships between observables.

The Telescope Array (TA) located in the high desert of Utah, USA, is the largest UHECR observatory in the Northern Hemisphere. It combines Fluorescence Detectors (FD) for observing air shower longitudinal development and Surface Detectors (SD) for measuring lateral particle distribution at the ground [3, 4]. FD provides more accurate primary particle reconstruction, but operates only 10% of the time due to clear and moonless night requirements, limiting event detection, especially at high energies. Standard SD reconstruction relies on the arrival times of the shower front, determined by the leading edge of the pulse from each counter, and the total signal charge, calculated by integrating the signal over time [1], without using the detailed time structure of the signals. DNNs can incorporate time-resolved signals to improve accuracy and recover subtle parameters like  $X_{\max}$  and mass [5–10], effectively extending FD-like capabilities beyond its limited duty cycle.

In this contribution, we present a DNN-based reconstruction that utilizes time-resolved signals in the form of two time traces recorded by the two scintillator layers of each surface detector. The DNN is trained on Monte Carlo (MC) simulations for four types of primaries (p, He, N, Fe). It demonstrates improved resolution for energy reconstruction, core position, and comparable performance for directional reconstruction. Using TA hybrid data, we validate that the DNN performs well on real data and provides results compatible with the established standard reconstruction approach.

## 2. Neural network architecture

We use a DNN that follows the AixNet architecture originally developed by the Auger Collaboration [7–10], with minor modifications to process TA data. The overall structure is illustrated in Fig. 1. The network processes input data in several stages, beginning with the time traces encoder. This encoder extracts features from two 128-length time traces recorded by each surface detector in the  $7 \times 7$  detector array. The encoder consists of three 3D convolutional layers, each followed by a ReLU activation, with a kernel size of (7,1,1), stride of (4,1,1), and zero padding, reducing the time dimension to one, which is then removed by reshaping. The channel dimensions change according to each layer's input and output settings.

The core of the network processes detector-level features, such as arrival times, total signals, detector statuses, and x, y, z coordinates, which are combined into a single tensor with dimensions (8,7,7) representing integral features. The output from the time traces encoder is concatenated with this feature tensor along the feature dimension. The resulting tensor is then passed through the spatial correlation encoder, consisting of multiple blocks of separable convolution layers. Sepa-

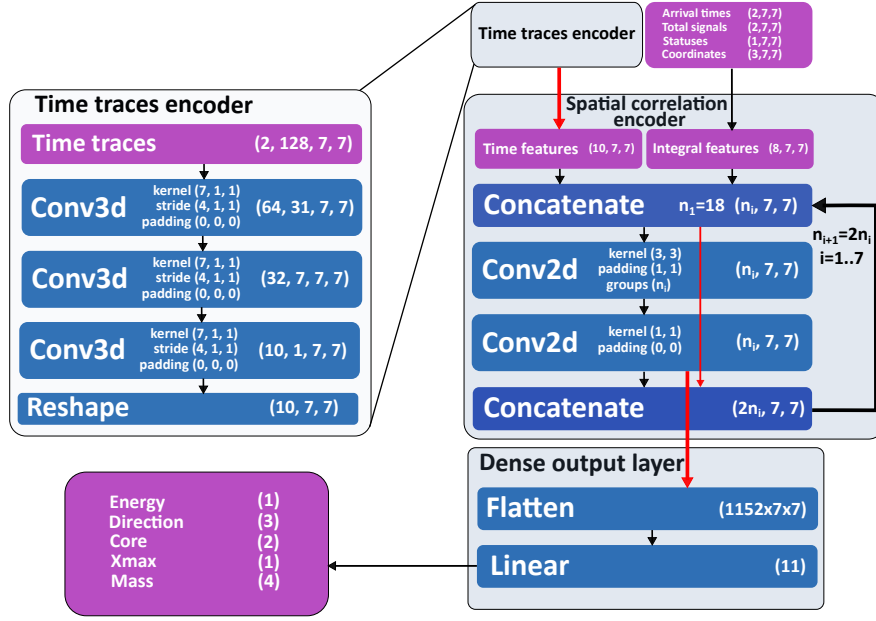


**Figure 1:** Schematic representation of the neural network architecture. Residual connections and layer transitions are highlighted with red arrows.

rable convolutions reduce parameters and computation compared to standard convolutions while preserving spatial and cross-channel correlations. Each block uses two stacked 2D convolutional layers. The first convolution processes each detector's feature map separately with a (3,3) kernel and (1,1) padding, preserving spatial dimensions. The second convolution operates along the feature dimension. Both layers are followed by ReLU activations.

A residual connection is applied by concatenating the block's output with its input, effectively doubling the feature dimension. The residual connections significantly improve performance of the DNN. This process is repeated for 7 blocks, except for the final one, where the residual connection is omitted. The final output is passed directly to the dense output layer, which flattens the feature representation and maps it to the 11-dimensional target vector through a linear transformation.

### 3. Input preprocessing

To ensure consistency and robustness of DNN training and inference, several preprocessing steps are applied, including normalization, transformation, and masking. Arrival times are normalized by subtracting the mean of active detectors and dividing by the standard deviation across all events, with inactive detectors set to zero. Time traces are summed over 128 bins to get the total signal, then transformed using  $\log(1+x)$  and scaled by a factor of 10. The total signal undergoes the same  $\log(1+x)$  transformation and is normalized using a fixed mean and standard deviation obtained from a Monte Carlo dataset, ensuring uniform normalization across datasets.

Spatial information is standardized by normalizing the detector coordinates so that the  $7 \times 7$  tile fits within a square where  $x$  and  $y$  range from  $[-1, 1]$ , achieved by dividing by  $1200 \times 3$  meters. The  $z$ -coordinate is scaled by dividing by  $1200 \times 3$  meters as well. An additional input encodes the status of each detector, assigning a value of 1 for active detectors and 0 for inactive or missing ones.

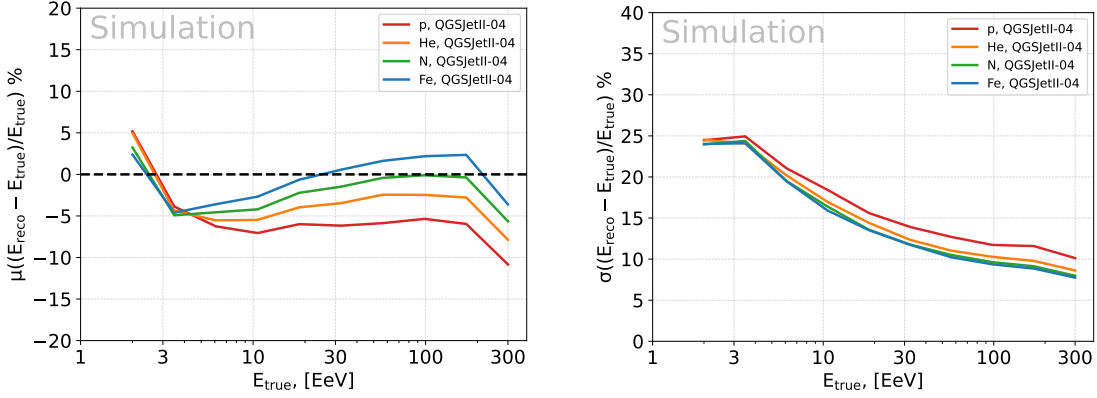


**Figure 2:** Bias (left) and resolution (right) of DNN energy reconstruction for events that passed quality cuts and simulated with QGSJetII-04 for different primary particles.

For training and inference,  $7 \times 7$  tiles of detectors, centered on the detector with the strongest total signal, are used. A larger  $9 \times 9$  tile size was tested but did not improve accuracy. The central detector often saturates, distorting the waveform and affecting measurements of the total number of particles. Also, CORSIKA simulations use thinning, with subsequent dethinning causing inaccuracies near the core. To mitigate this, the central detector in the  $7 \times 7$  tile is set to zero during training and inference. While this slightly reduces reconstruction accuracy on Monte Carlo datasets, it improves generalization to real Telescope Array data by making the total signal more consistent across datasets.

#### 4. Monte Carlo datasets

The DNN was trained and tested using Monte Carlo simulations generated with CORSIKA 7.3500 and the QGSJetII-04 hadronic interaction model. The dataset includes proton, helium, nitrogen, and iron primaries with 0.5 million events per species. Air showers are simulated in 26 logarithmically spaced energy bins in the range from 1 EeV to 300 EeV, following an  $E^{-1}$  spectrum. Each bin contains 1000 CORSIKA showers with arrival directions sampled isotropically for zenith angles below 70 degrees. Showers are resampled 20 times by rotating them, rescaling their energy, and using the TA simulation framework to model realistic detector response, including electronics, detector status, and background effects [1, 11]. The test dataset contains another 0.5 million events with the same characteristics as the training data. The results are presented for events that pass the standard quality cuts for the analysis of the spectrum. [1, 11]. To assess the model's robustness across varying hadronic interactions, two additional datasets based on the QGSJetII-03 and Sibyll 2.3d hadronic interaction models for proton and iron primaries were used.

#### 5. Energy reconstruction

The performance of DNN energy reconstruction is first evaluated on a test dataset with the same energy spectrum, composition, and hadronic model QGSJetII-04 as for the training data. The evaluation is based on the bias and resolution of the relative reconstruction error. Results are shown for events that pass standard spectral quality cuts.

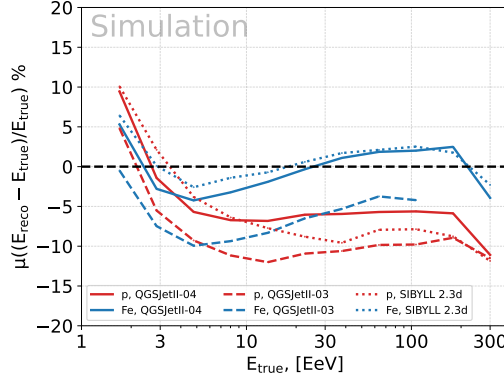


**Figure 3:** Comparison of DNN energy reconstruction biases across different hadronic interaction models for events that passed quality cuts.

The bias of DNN energy reconstruction is shown in the left panel of Fig. 2. Bias values vary with the primary particle type and are generally centered around zero, with a slight tendency toward negative values. The upward shift at low energies and the slight downward bending at the highest energies are edge effects, as the DNN is trained within the 1–300 EeV range and does not predict values outside this interval. Since the reconstruction bias depends on both the hadronic interaction model and the primary mass, it should ultimately be corrected through calibration against hybrid event data.

The energy resolution is shown in the right panel of Fig. 2. For protons, the resolution decreases from 25% at low to 10% at high energies, while for iron, it improves from 23% to 7%, giving iron a 2–3% better resolution overall. Other elements fall between these values, generally closer to iron. The largest resolution difference is between protons and heavier nuclei, but the resolution's dependence on particle type is weaker than for the bias.

Fig. 3 shows the biases for proton and iron across different hadronic interaction models. The DNN trained on QGSJetII-04 produces a negative bias when reconstructing proton and iron events simulated with QGSJetII-03. The Sibyll 2.3d results are similar to QGSJetII-04 but with slightly larger biases.

The left panel of Fig. 4 compares the energy reconstruction resolution of the DNN trained on QGSJetII-04, evaluated on datasets generated with QGSJetII-03 and Sibyll 2.3d. The resolution shows only a weak dependence on the interaction model, with a slight degradation for models not used in training. This suggests that the DNN generalizes well across different hadronic interaction models.

The right panel of Fig. 4 compares the energy reconstruction resolution of the DNN with the standard method on a dataset generated with QGSJetII-03, ensuring a consistent comparison since the standard method is tuned for this model. The resolution is evaluated across two energy ranges reported by TA collaboration [1, 11]. The DNN improves resolution by approximately 30%. It is a significant result, because resolution is generally more challenging to account for in energy spectrum reconstruction than bias. The improved resolution directly enhances the precision of energy measurements.

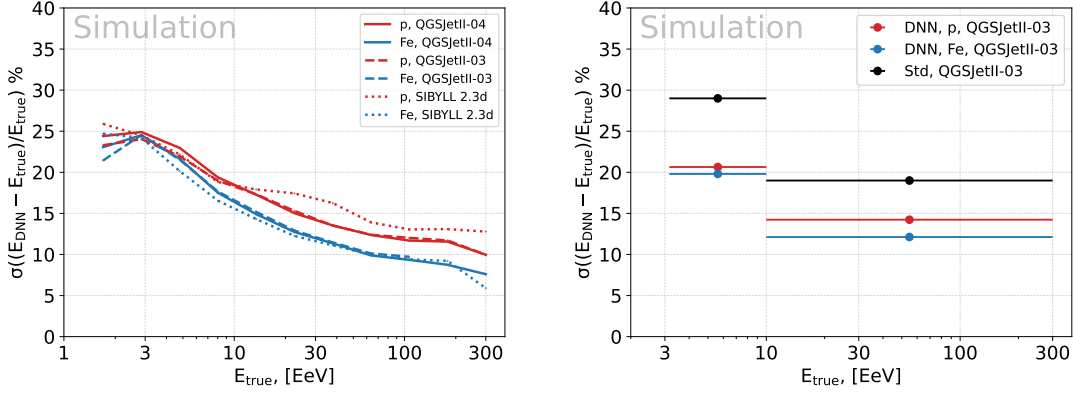


**Figure 4:** Resolution of DNN energy reconstruction for events that passed quality cuts. Left: Comparison of resolution across different hadronic interaction models. Right: Comparison of DNN and standard energy reconstruction resolution for events simulated with QGSJetII-03.

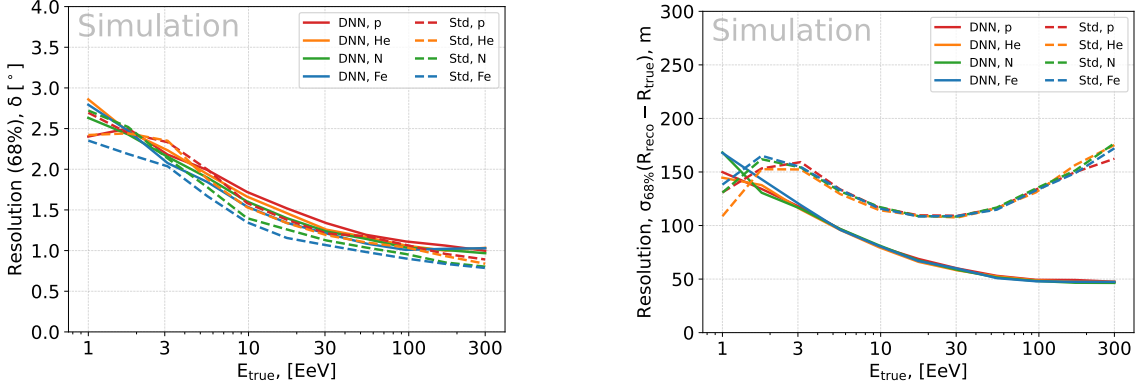


**Figure 5:** Angular resolution of DNN and standard reconstruction.

**Figure 6:** Resolution of shower core position reconstruction for the DNN and standard methods.

## 6. Reconstruction of direction and core position

Fig. 5 shows the angular resolution of the directional reconstruction, defined as the 68th percentile of the angular distance between the reconstructed and true directions. Both DNN and standard reconstruction tend to have better resolution with increasing nuclear mass as heavier particles produce a stronger signal. The DNN resolution is slightly worse typically by no more than 0.2 degrees over most of the energy range. Fig. 6 presents the resolution of the reconstructed shower core position, defined as the 68th percentile of the distance between the reconstructed and true core locations. The resolution shows little to no dependence on the primary particle type for both the DNN-based and standard reconstruction methods. The standard reconstruction achieves a resolution between 100 and 150 meters, while the DNN improves this to 50 meters at high energies, reducing the resolution by a factor of 1.5–2.

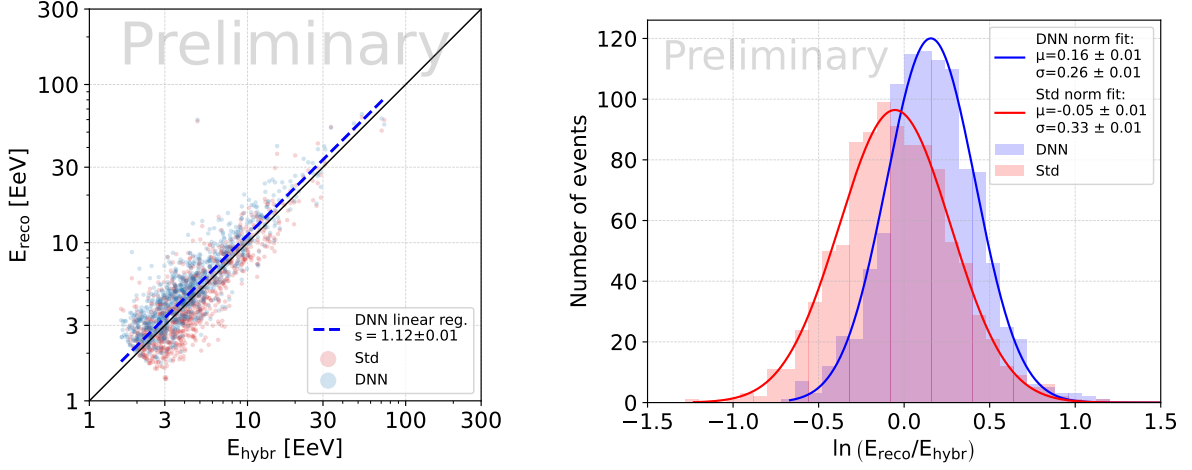


**Figure 7:** Left: Comparison of standard and DNN energy reconstruction on the TA hybrid events dataset. Right: Histograms over  $\ln(E_{\text{reco}}/E_{\text{hybr}})$  and normal distribution fits to them. The DNN results are shown before applying the scaling factor, while standard reconstruction results are shown with a scaling factor of  $1/1.27$  applied.

## 7. Validation on TA hybrid data

To evaluate the DNN energy reconstruction on real data, we compare it with the standard method using hybrid data detected by both SD and FD. The hybrid dataset includes 3656 events detected over 9 years from May 27, 2008 to November 28, 2017. The scatter plot of 1033 events passed standard quality cuts in the left panel of Fig. 7 shows that the DNN reconstructs energy with performance comparable to the standard method, validating its ability to handle real data. A linear regression fit shows a bias of 1.12, so the calibration factor for DNN reconstructed energies is  $E_{\text{hybr}} = E_{\text{DNN}}/1.12$ . For consistency, we assumed an energy-independent bias, allowing direct comparison with standard reconstruction. The standard method's calibration factor of  $1/1.27$  is already applied in the figure. Note that DNN's calibration factor is not universal, as different models, even trained on the same dataset, may result in slightly different factors. Right panel of Fig. 7 shows distributions of events around diagonal line with normal distribution fits. It is seen that DNN gives resolution of 30% compared to standard reconstruction resolution of 39% (see formula (5.17) in [1]).

## 8. Conclusion

We present a DNN approach for energy, direction, and core position reconstruction applied to simulated SD, and energy reconstruction for real hybrid TA data. Using MC datasets, we observe a 30% improvement in energy resolution, a factor of 1.5–2 improvement in core position reconstruction, and performance in directional reconstruction comparable to the standard method. DNN energy reconstruction is robust to changes in hadronic interaction models, with a maximal bias difference of 7% between QGSJetII-03 and QGSJetII-04 and weak dependence for resolution. DNN is validated on real hybrid TA data, demonstrating 23% of relative improvement in resolution.

## 9. Acknowledgments

AP and AF acknowledge support from the Academia Sinica Grand Challenge Seed Grant under Grant No. AS-GCS-113-M04 and the Academia Sinica Grid Computing Centre (ASGC) under Grant No. AS-CFII-112-103.

## References

- [1] Dmitri Ivanov. “Energy spectrum measured by the telescope array surface detector”. PhD thesis. Rutgers U., Piscataway, 2012.
- [2] Alexander Aab et al. “Measurement of the cosmic-ray energy spectrum above  $2.5 \times 10^{18}$  eV using the Pierre Auger Observatory”. In: *Phys. Rev. D* 102.6 (2020), p. 062005. doi: [10.1103/PhysRevD.102.062005](https://doi.org/10.1103/PhysRevD.102.062005). arXiv: [2008.06486](https://arxiv.org/abs/2008.06486) [astro-ph.HE].
- [3] H. Tokuno et al. “New air fluorescence detectors employed in the Telescope Array experiment”. In: *Nucl. Instrum. Meth. A* 676 (2012), pp. 54–65. doi: [10.1016/j.nima.2012.02.044](https://doi.org/10.1016/j.nima.2012.02.044). arXiv: [1201.0002](https://arxiv.org/abs/1201.0002) [astro-ph.IM].
- [4] T. Abu-Zayyad et al. “The surface detector array of the Telescope Array experiment”. In: *Nucl. Instrum. Meth. A* 689 (2013), pp. 87–97. doi: [10.1016/j.nima.2012.05.079](https://doi.org/10.1016/j.nima.2012.05.079). arXiv: [1201.4964](https://arxiv.org/abs/1201.4964) [astro-ph.IM].
- [5] D. Ivanov et al. “Using deep learning to enhance event geometry reconstruction for the telescope array surface detector”. In: *Mach. Learn. Sci. Tech.* 2.1 (2021), p. 015006. doi: [10.1088/2632-2153/abae74](https://doi.org/10.1088/2632-2153/abae74). arXiv: [2005.07117](https://arxiv.org/abs/2005.07117) [astro-ph.HE].
- [6] O. Kalashev et al. “Deep learning method for identifying mass composition of ultra-high-energy cosmic rays”. In: *JINST* 17.05 (2022), P05008. doi: [10.1088/1748-0221/17/05/P05008](https://doi.org/10.1088/1748-0221/17/05/P05008). arXiv: [2112.02072](https://arxiv.org/abs/2112.02072) [astro-ph.IM].
- [7] M. Erdmann, J. Glombitza, and D. Walz. “A deep learning-based reconstruction of cosmic ray-induced air showers”. In: *Astropart. Phys.* 97 (2018), pp. 46–53. doi: [10.1016/j.astropartphys.2017.10.006](https://doi.org/10.1016/j.astropartphys.2017.10.006). arXiv: [1708.00647](https://arxiv.org/abs/1708.00647) [astro-ph.IM].
- [8] Alexander Aab et al. “Deep-learning based reconstruction of the shower maximum  $X_{max}$  using the water-Cherenkov detectors of the Pierre Auger Observatory”. In: *JINST* 16.07 (2021), P07019. doi: [10.1088/1748-0221/16/07/P07019](https://doi.org/10.1088/1748-0221/16/07/P07019). arXiv: [2101.02946](https://arxiv.org/abs/2101.02946) [astro-ph.IM].
- [9] Alexander Aab et al. “Extraction of the muon signals recorded with the surface detector of the Pierre Auger Observatory using recurrent neural networks”. In: *JINST* 16.07 (2021), P07016. doi: [10.1088/1748-0221/16/07/P07016](https://doi.org/10.1088/1748-0221/16/07/P07016). arXiv: [2103.11983](https://arxiv.org/abs/2103.11983) [hep-ex].
- [10] A. Abdul Halim et al. “Inference of the Mass Composition of Cosmic Rays with Energies from 1018.5 to 1020 eV Using the Pierre Auger Observatory and Deep Learning”. In: *Phys. Rev. Lett.* 134.2 (2025), p. 021001. doi: [10.1103/PhysRevLett.134.021001](https://doi.org/10.1103/PhysRevLett.134.021001). arXiv: [2406.06315](https://arxiv.org/abs/2406.06315) [astro-ph.HE].
- [11] T. Abu-Zayyad et al. “CORSIKA Simulation of the Telescope Array Surface Detector”. In: (Mar. 2014). arXiv: [1403.0644](https://arxiv.org/abs/1403.0644) [astro-ph.IM].